HHS Public Access

Author manuscript

Bioinspir Biomim. Author manuscript; available in PMC 2022 July 15.

Published in final edited form as:

Bioinspir Biomim. ; 16(5): . doi:10.1088/1748-3190/ac0a33.

Mechanical Evaluation of 3D Printed Biomimetic Non-Euclidean Saddle Geometries Mimicking the Mantis Shrimp

Tara E. Mensch[a], **Elizabeth A. Delesky**[b], **Robert W. Learsch**[b], **Kyle E. O. Foster**[b], **Sai Kaushik Yeturu**[b], **Wil V. Srubar III**[b,c], **Garret Miyake**[a,†]

[a]Department of Chemistry, Colorado State University, Fort Collins, Colorado 80523, United States,

[b]Materials Science and Engineering Program, ECOT 441 UCB 428, Boulder, Colorado 80309-0428 USA,

[c]Department of Civil, Environmental, and Architectural Engineering University of Colorado Boulder, ECOT 441 UCB 428, Boulder, Colorado 80309-0428 USA,

Abstract

Engineering design has drawn inspiration from naturally occurring structures to advance manufacturing processes and products, termed biomimetics. For example, the mantis shrimp, order *Stomatopoda*, is capable of producing one of the fastest appendage strikes in the world with marginal musculoskeletal displacement. The extreme speed of the mantis shrimp's raptorial appendage is due to the non-Euclidean hyperbolic paraboloid (*i.e.*, saddle) shape within the dorsal region of the merus, which allows substantial energy storage through compression in the sagittal plane. Here, investigation of 3D printed synthetic geometries inspired by the mantis shrimp saddle geometry has revealed insights for elastic energy storage (*i.e.*, spring-like) applications. Saddles composed of either a *stiff* or a *flexible* resin were investigated for spring response to explore the geometric effects. By modulating the saddle geometry and testing the spring response, it was found that, for the *stiff* resin, the spring constant was improved as the curvature of the contact and orthogonal faces were maximized and minimized, respectively. For the *flexible* resin, it was found that the spring constant increased by less than 250 N/mm as the saddle geometry changed, substantiating that the flexible component of mantis saddles does not contribute to energy storage capabilities. The geometries of two saddles from the mantis shrimp species *Odontodactylus scyllarus* were estimated and exhibited similar trends to manufactured saddles, suggesting that modulating saddle geometry can be used for tailored energy storage moduli in spatially constrained engineering applications.

Keywords

biomimetics; biomimicry; additive manufacturing; 3D printing; mantis shrimp

[†]Corresponding Author, garret.miyake@colostate.edu.

1.0 Introduction

1.1 Non-Euclidean geometry and the mantis shrimp

Non-Euclidean geometry is pervasive in nature: from fungi hyphae [1], to coral colonies [2], to flea joints [3]. Organisms often evolve and develop non-Euclidean geometries to optimize solutions to complicated problems, including maximizing surface area exposure while minimizing volume [2] or improving energy storage within a confined space [4]. Non-Euclidean geometries maximize efficiency by minimizing energetic and material costs [5].

A biological study has found that some species from the order *Stomatopoda*, commonly known as mantis shrimp, are able to accelerate their raptorial appendage to lethal velocities (14–23 m/s) due to the non-Euclidean hyperbolic paraboloid (*i.e.*, saddle) shape within its shoulder [4]. The compression of the saddle in the sagittal plane direction allows substantial energy storage and rapid dissipation for fracturing the tough exoskeletons of its prey [4]. The mantis shrimp saddle demonstrates a compelling non-Euclidean geometry that optimizes elastic energy storage within spatial constraints.

The mantis shrimp saddle is a bilayer composite with a gradient of inorganic minerals dispersed in an organic matrix from the upper to lower regions. The organic-inorganic composite enables exceptional energy storage due to the stiff outer later, and the flexible inner layer prevents stress concentration and failure [6, 7]. The upper region consists of highly mineralized amorphous calcium carbonate and amorphous calcium phosphate dispersed in an organic chitin matrix, allowing for high compressive loading. The lower region is comprised of flexible chitin, a variety of proteins—including some that are reminiscent of elastin, which facilitates elongation—and a small quantity of amorphous calcium carbonate [6, 7]. Mantis shrimp saddles have been shown to maintain approximately the same spring constant within species, regardless of sex, size, and morphology due to varied mineralization of individual saddles [8, 9]. It has been hypothesized that the organic-inorganic material composition gradient has adapted over time to improve load-bearing capabilities of the saddle, with flexible organic components that provide mobility, energy dissipation, and cyclic durability, while the stiff inorganic components provide extraordinary potential energy storage [8]. Understanding how to modulate the individual components of the specialized merus (first segment of the raptorial appendage) region in the mantis shrimp will facilitate replication in future synthetic engineering systems. As there are no muscle attachments to the saddle [10], and it exhibits a significant contribution (20%) to the acting mechanism in the mantis shrimp's raptorial strike, understanding the contribution of saddle geometry to the spring constant provides a facile first step for translating the power amplification system found in the mantis shrimp to an engineered replicate.

Saddles vary with species and are morphology dependent. As morphology has changed with evolution, looking at different geometries is a crucial step for engineering a complex modular system to ensure efficiency of the full system. It is hypothesized that the saddle provides a flexible (low mineralization) yet strong (20% of spring constant) response during the load phase and can reduce buckling due to its hyperbolic paraboloid shape [10]. Engineering systems often utilize various, non-traditional geometries [10,11] to achieve a

spring-like response. Rapid, cyclic actions require elasticity of the appendage, so while the energy storage is low, flexibility of the component is necessary for repeatability [12].

1.2 Biomimetics

The field of biomimetics uses nature as inspiration by emulating naturally occurring shapes, structures, and functions to improve engineering design for modern purposes [13, 14]. Biomimetics has provided a wide variety of solutions at every scale of the natural hierarchy, from nano-scale patterning [14–19] to macro-scale functional structures [20, 21] as well as electroactive polymers used as smart artificial muscles [22,23]. Direct replication of nature has led to the development of elegant solutions to complex problems, such as structural stability from honeycomb architecture [24–26], improved aerodynamics from kingfisher beaks [20], and shock absorption from woodpecker skull anatomy [27, 28].

Additive manufacturing (AM), or 3D printing, has recently gained momentum as a fabrication tool leveraged in both research and industrial applications [29, 30]. AM has enabled facile production of singular or batched custom-made objects [31, 32] and can expedite manufacturing [33, 34]. Together, biomimicry and AM have enabled replication of complicated natural designs for engineering applications in diverse fields, such as scaffold-based tissue engineering [29, 35, 36], facile fabrication of complex microfluidics [29], and large-scale infrastructure [13, 37]. This offers a unique method to fabricate intricate, non-linear morphologies, like the non-Euclidean geometries of the mantis shrimp saddle. The output of spring driven systems are governed by the inherent stiffness of the spring material, as well as being dictated by the spring geometry [11]. The saddle geometry has a large impact on spring constant, shown by Lipson *et al.* [13], by a decrease when the saddle is severed. As the spring constant doesn't depend on length or size of the merus region [13], looking at the spring constant will be a useful comparison for engineering applications. Understanding how geometry affects component performance is a critical step in optimizing modular, potentially tunable synthetic systems. Although the fabrication of multimaterial parts through 3D printing remains challenging, this work seeks to investigate the unique properties of the saddle geometry for homogeneous parts printed from either a stiff or flexible resin to gain insight into modifications of the saddle dimensions on spring-like performance.

1.3 Scope of work

As spring-like behavior is geometry and material dependent, we focus on the questions: (1) what is the effect of geometry on the spring-like performance of the saddle for the same material composition and (2) what is the effect of material on the spring-like performance of the saddle for the same geometries? It is anticipated that high spring constants will be compromised within spatial constraints, and will be altered depending on material. A matrix of hyperbolic paraboloid geometries, inspired by the non-Euclidean saddle from the order *Stomatopoda*, were systematically manufactured *via* AM. Isotropic mechanical performance of the print resin was investigated using symmetric saddle geometries printed in orthogonal orientations. Saddles were mechanically compressed to determine the relationship between saddle geometry and the resulting spring constant. The effect of resin stiffness on the spring constant of manufactured saddles was explicitly investigated by testing two different resin

formulations with identical geometry saddles. Finally, saddle geometries from the species *Odontodactylus scyllarus* were estimated and compared to experimental results of the 3D-printed geometries investigated herein.

2.0 Materials and Methods

2.1 Materials

RS-F2-GPCL-04 resin (termed the *stiff* resin herein), RS-F2-TOTL-05 resin (termed the *flexible* resin herein), and FORM 2 resin tanks were purchased from Formlabs. Isopropyl alcohol was purchased from Fisher Scientific and used without additional purification. A saddle from the peacock mantis shrimp, *Odontodactylus scyllarus*, was obtained from a private eBay vendor.

2.2 Experimental Methods

2.2.1 3D Printing File Design—Saddles with systematically varied geometry were designed utilizing Equation 1:

$$\frac{x^2}{\alpha} - \frac{y^2}{\beta} = z \qquad \text{Eq. 1}$$

Equation 1 is given as the cartesian equation for a three-dimensional hyperbolic paraboloid, with added variables α and β to adjust the magnitude of curvature in the x and y dimension. The coefficients α and β were varied incrementally from 0.25 to 4 (α = {0.5, 1 2, 4} and β = {0.25, 0.5, 1, 2}), while the geometric footprint was confined to a 2” by 2” square in the x-y plane, resulting in a matrix of saddles with different sizes and shapes, as summarized in Table 1.

The mathematical equations for each saddle geometry were plotted using SurfX3D with bounds from −1 to 1 in both the x and y dimensions and without bounds in the z dimension. Saddle geometries were saved using a .dxf extension and converted to a 3D part using Solid Works. Meshmixer was used to extrude the print with a thickness of 2.2 mm. PreForm was used to lay multiple prints on a plate and communicate prints to the Formlabs Form2 3D printer.

2.2.2 Saddle Printing—All 3D printing was performed with an unmodified Form 2 SLA 3D printer (Formlabs). Resin prints were made using a 0.05 mm print resolution and an infill density of 100%. After print completion, Formlabs Form2 protocol was followed. Briefly, printed saddles were placed in a tank of isopropyl alcohol for 15 mins, followed by another 15 min isopropyl alcohol wash in a separate tank to remove any residual uncured resin. Print supports were manually removed and the saddles were stored away from UV light at ambient temperature until mechanical testing could be performed. Printed saddles using *stiff* and *flexible* resin are shown in Figure S1. The *stiff* resin was used to print all sample geometries in Table 1. The *flexible* resin was used to print geometries with β = 0.25 and varied α (α = {0.5, 1, 2, 4}).

2.2.3 Mechanical Compression Testing—Mechanical compression testing was performed on an Instron 5966 Universal (Tension/Compression) Testing Machine. A 10 kN load cell was used to test all samples. All tests were displacement-controlled and conducted according to ASTM D695 [38]. Samples were loaded as shown in Figure 1c, parallel to the plates. This loading was chosen due to its similarity to the biological compression of the mantis shrimp saddle, in which applied longitudinal force induces transversal expansion [7]. A standard speed of 0.022 mm/s was used for sample compression. Data collection started prior to contact of the top plate with the sample to ensure all relevant data were collected. Data acquisition continued until permanent damage was evident, and each test sample was digitally filmed during compression to ensure accuracy. Data corresponding to elastic deformation in the linear region were used for determining the spring constant of samples. The reported spring constants were averaged from 5 replicates per sample geometry.

2.2.3.1 Print Resin Isotropy: Isotropy of the print resin was investigated by manufacturing saddles with a symmetric design ($\alpha = \beta$) to ascertain if print orientation of the resin had an impact on spring constant. Compression testing was performed parallel to the print direction (with regard to the parabola defined by α) and orthogonal to the print direction (with regard to the parabola defined by β), as visualized in Figure 1a and Figure 1b respectively. To ensure resin isotropy with different geometries, three different symmetric geometries were tested ($\alpha = \beta = 0.5$, $\alpha = \beta = 1$, $\alpha = \beta = 2$). Samples were tested in triplicate. The significance of saddle parameters ($\alpha = \beta$) and compression testing orientation on the saddle spring response was tested using two-factor ANOVA, with the dependent variables log transformed to satisfy normality and homoscedasticity. For main effects, significance was set *a priori* to $p < 0.05$.

2.2.3.2 Spring Constant Determination: Once isotropy was confirmed, α was arbitrarily chosen as the reference for saddle orientation for further compression testing (Table 1). Prints were oriented such that the parabola defined by α was under compression, as indicated in Figure 1c.

The Hookean spring constant (k), or stiffness, of an object is defined as the ratio of the load (F) over the corresponding displacement (δ), as given in Equation 2:

$$k = \frac{F}{\delta} \quad \text{Eq. 2}$$

For each measurement, the data were transformed using a moving average to eliminate noise. The spring constant was determined by taking the slope between 25%–75% of the displacement in the linear elastic region for the compression load-displacement response. The end of the linear elastic region was identified as a deviation of more than 5% from the slope taken within the linear region. Plots of force versus displacement used to calculate spring constant from the linear elastic region in *stiff* resin saddles are shown in Figure S2. Non-linearity in plots shown in Figure S2 is likely due to plotting samples of the same geometry using uniform displacements, however, calculations were made at 25%–75% linear displacement to ensure accuracy. The significance of saddle parameters (α and β) on

the saddle spring response was tested using one-factor ANOVA in MATLAB, with the dependent variable log transformed to satisfy normality and homoscedasticity. For main effects, significance was again set *a priori* to $p < 0.05$.

2.3 Saddle Geometry for Biological Samples

The native saddle geometry of the peacock mantis shrimp *Odontodactylus scyllarus* was investigated for comparison to manufactured saddle geometries. To measure the saddle geometry, a similar method based on Tadayon *et al.*, who generated a microCT scan of a saddle from *Odontodactylus scyllarus* and fit parabolas to the saddle geometry [6], was employed. A Nikon 1 V1 digital camera was used to image the *Odontodactylus scyllarus* saddle in both the longitudinal and transverse directions. The imaged saddle was used to fit parabolas to the saddle geometry (Figure S3). Geometric constants for α (longitudinal) and β (transverse) were determined as the absolute value of the inverse of the x coefficient of the parabolic equations (Table S1).

3.0 Results and Discussion

3.1 Saddle Resin Isotropy

As AM occurs in layers, mechanical response may be influenced by applied load relative to print direction. Two-way ANOVA was used to confirm resin isotropy independent of printing direction. Compression testing orientation was shown to not significantly impact the spring response of printed saddles. Each tested geometry (where $\alpha = \beta$); 0.5, 1, and 2 had spring responses distinct from each other grouping ($p < 0.05$). When comparing within the geometry grouping (Figure 2), saddles printed in the parallel and orthogonal directions were not statistically different from one another ($p > 0.05$) (Table S2), indicating isotropy with regard to print orientation (Figure 2). Resin isotropy is attributed to interlayer crosslinking during the SLA printing process, which renders the manufacturing direction unimportant to resin performance [39, 40].

3.2 Saddle Geometry and Spring Constants

Spring constants for *stiff* resin saddles shown in Table 1 varied over four orders of magnitude (from 0.659 N/mm to 1740 N/mm) due to changes in geometry, as seen in Figure 3 and summarized in Table 2. The spring constant data for *stiff* saddles were log-transformed to satisfy normality and homoscedasticity required for a one-way ANOVA. Each of the geometry dependent spring responses was statistically different from one another ($p < 0.05$) (Table S2), with the exception of three specimen groups (notation – (α, β)): (4, 0.5) and (4, 1); (2, 0.5) and (4, 2); (0.5, 0.25), (2, 2), and (1, 0.5). Figure 3 demonstrates that the spring constant increased with α for each saddle geometry with a constant β coefficient. Table 2 summarizes the determined spring constants, with error shown being calculated from error between samples tested. Notably, for all values of β, as α increased from 0.5 to 1 the spring constant increased by an order of magnitude. It is hypothesized that, because increasing α reduces the radius curvature between the opposite faces of the saddle, geometry-induced rigidity at the localized points in contact with the applied force is observed [41, 42]. The geometry-induced rigidity increases the spring constant under load-bearing conditions.

For each constant value of α, decreasing β improved the performance of the saddle (Figure 3). For example, geometries with α = 1, the largest β coefficient (β = 2) exhibited the smallest spring constant at 1.96 ± 0.242 N/mm, whereas the smallest β coefficient (β = 0.25), exhibited the largest spring constant at 245 ± 31.2 N/mm. Data show that the spring constant can be increased by minimizing β, as smaller β values withstand higher levels of strain in the dimension orthogonal to the applied load.

The largest spring constants were achieved by increasing α and reducing β. Increasing α maximized curvature of the saddle faces in contact with the applied load, causing geometry-induced rigidity that increased the spring constant. Decreasing β minimized the curvature of the faces and allowed uniform displacement over the saddle geometry. Values for α and β were estimated from two biological specimens and were compared to experimental data. The saddle geometries for *Odontodactylus scyllarus* (one dried biological specimen and one microCT scan) were α = 16.39 and β = 2.11, and α = 13.51 and β = 7.81, respectively, which corroborates the trend of high α values. It is expected that the β values for *Odontodactylus scyllarus* were not 'small' because the saddles occupy more space in the z-dimension as β is decreased (Table 1), and there is limited space in the z-dimension in the mantis shrimp merus. The β values for *Odontodactylus scyllarus* differed from the optimal, minimized β values of the manufactured saddles since manufactured saddles lack spatial constraints in the z-direction, thus allowing greater stress distributions over larger surface area. It is suspected that the biological saddle geometry developed to maximize stiffness under spatial constraints while maintaining feasible demands for shrimp musculature to deform the saddle for energy storage. In order to assess the energy storage of each sample, the elastic potential energy storage for each sample was calculated using Equation S1 and a linear displacement of 0.1 mm in accordance with the average displacement of the mantis shrimp saddle when compressed [43]. Calculated values of elastic potential energy storage of *stiff* saddles is given in Table S3. Values shown in this table follow the same trends as spring constants, shown in Table 2 due to the relationship between spring constant, displacement, and energy storage.

Tadayon *et al.* tested 25 biological saddles from two species of mantis shrimp (*Odontodactylus scyllarus and Harpiosquilla harpax*) in compression and found a spring constant of 143.6 ± 31.8 N/mm [6], similar to the spring constant of the *stiff* resin geometry α = 0.5 and β = 0.25 (106 ± 12.2 N/mm). However, for a similar *k*, the geometry differs due to the biological complexities that are unable to be mimicked using the single layer resin formulations used in this study. The α and β for *Odontodactylus scyllarus* were used to generate saddles in SurfX3D (Figure S4), and the generated saddles most resembled the saddle geometry α = 4 and β = 2. The difference in the geometry to spring constant relationship is likely due to the complex composition of the biological saddle that has a dispersed mineral phase in a proteinaceous matrix, allowing for improved stress distributions between the material phases [7].

By varying the values of α and β, the multiaxial deformation can be tuned to account for material and spatial constraints, allowing for the optimization of performance within confined parameters. The customizability offers the potential for saddles in mechanical applications with material or spatial constraints.

3.3 Effect of Resin on Saddle Spring Constant

Saddles printed from the *flexible* resin were tested at the minimum β coefficient for improved performance, as saddles printed from the *stiff* resin showed that reducing the face curvature increased saddle spring constants. The spring constants for both print resins were compared with two-way ANOVA, with the data log transformed to satisfy normality and homoscedasticity. The influence of resin type was apparent (Table 3): the *flexible* resin consistently exhibited lower spring constants than the *stiff* resin at comparable saddle geometries ($p < 0.05$).

As expected, *flexible* resin saddles exhibited lower spring constants than the *stiff* resin saddles, which were by an order of magnitude for α values of 1, 2, and 4 (Table 3). For the *stiff* resin saddles, *k* increased as α increased – notably, the *flexible* resin saddles did not follow the same trend, i.e., *k* was larger for $\alpha = 1$ than $\alpha = 2$ (91.1 vs. 68.8 N/mm, respectively). These results likely occurred due to the minimal relationship between geometry and spring constant when using *flexible* resin, as energy was dissipated during compression rather than being stored. Overall, the spring constant for *flexible* resin saddles increased <100 N/mm as α increased from 0.5 to 4, compared to *stiff* resin saddles, which increased >2,000 N/mm over the same geometry range. While the *flexible* resin data points are statistically different (Table S2), the spring constant for the *flexible* resin saddles appears to reach a plateau-like region when $\alpha \geq 1$ (Figure 4), suggesting that changes in geometry for the *flexible* resin have less influence on saddle performance in compression. These results support the hypothesis that the flexible layer of chitin and other proteinaceous material in the mantis shrimp saddle does not significantly contribute to energy storage.

4.0 Conclusions

In recent years, scientists have increasingly sought to use nature as inspiration by emulating naturally occurring shapes, structures, and functions to improve engineering designs. The junction of biomimicry and additive manufacturing (AM) enabled replication of complicated natural designs for engineering applications in various fields. Within the dorsal region of the merus of the mantis shrimp, a hyperbolic paraboloid (saddle) shape offers a novel alternative spring design that allows high energy storage from minimal compression due to a large spring constant, as according to equation 2.

A matrix of hyperbolic paraboloid geometries inspired by the non-Euclidean saddle from the order *Stomatopoda* was systematically manufactured using a *stiff* and a *flexible* resin and tested in compression for Hookean spring constants based on saddle shape. The effect of print orientation, saddle geometry, and saddle resin were investigated. Results indicate that the spring constant of the saddles was independent of print orientation, substantiating isotropic material behavior. For the *stiff* resin saddles, the largest spring constants were achieved by increasing geometric factor α and reducing geometric factor β. Increasing values of α reduced the curvature between the opposite faces of the saddle, invoking geometry-induced rigidity that increased the spring constant. Minimizing values of β increased the curvature of the faces in contact with the compressive load and allowed uniform displacement over the saddle geometry. As expected, the *flexible* resin saddles exhibited lower spring constants than the *stiff* resin saddles by an order of magnitude for

corresponding geometries. The *flexible* resin saddle spring constants appeared to reach a plateau with changes in geometry, indicating that shape does not influence the spring constant of these saddles in compression. Measurements of biological saddles from the mantis shrimp *Odontodactylus scyllarus* corroborated the trend for maximization of α to maximize spring constant; however, it appeared the minimization of β was compromised to account for spatial restraints. These findings show that geometry of non-Euclidean hyperbolic paraboloids can be altered to optimize spring constants for mechanical applications.

Supplementary Material

Refer to Web version on PubMed Central for supplementary material.

Acknowledgments

This research was made possible by the Department of Chemistry at Colorado State University. This research received financial support from the United States (US) National Science Foundation (Award Nos. CMMI-1727788 and CMMI-1634941), and the National Institutes of Health under Award R35GM119702. The authors appreciate Bret Boyle, Cameron Chrisman and Emily Mensch for their advice, assistance, and support in this work. This work represents the views of the authors and not necessarily those of the sponsors.

6.0 References

[1]. Matsuura S, & Miyazima S (1992). Self-affine fractal growth front of Aspergillus oryzae. Physica A: Statistical Mechanics and its Applications, 191(1–4), 30–34.

[2]. Anthony KRN, Hoogenboom MO, & Connolly SR (2005). Adaptive variation in coral geometry and the optimization of internal colony light climates. Functional Ecology, 19(1), 17–26.

[3]. Bennet-Clark HC, & Lucey ECA (1967). The jump of the flea: a study of the energetics and a model of the mechanism. Journal of Experimental Biology, 47(1), 59–76.

[4]. Patek SN, & Caldwell RL (2005). Extreme impact and cavitation forces of a biological hammer: strike forces of the peacock mantis shrimp Odontodactylus scyllarus. Journal of Experimental Biology, 208(19), 3655–3664.

[5]. Colorni A, Dorigo M, Maffioli F, Maniezzo V, Righini G, & Trubian M (1996). Heuristics from nature for hard combinatorial optimization problems. International Transactions in Operational Research, 3(1), 1–21.

[6]. Tadayon M, Amini S, Masic A, & Miserez A (2015). The mantis shrimp saddle: a biological spring combining stiffness and flexibility. Advanced Functional Materials, 25(41), 6437–6447.

[7]. Tadayon M, Amini S, Wang Z, & Miserez A (2018). Biomechanical Design of the Mantis Shrimp Saddle: A Biomineralized Spring Used for Rapid Raptorial Strikes. iScience, 8, 271–282. [PubMed: 30344051]

[8]. Patek SN, Rosario MV, & Taylor JRA (2013). Comparative spring mechanics in mantis shrimp. Journal of Experimental Biology, 216(7), 1317–1329.

[9]. Zack TI, Claverie T, Patek SN. (2009). Elastic energy storage in the mantis shrimp's fast predatory strike. Journal of Experimental Biology 212:4002–4009.

[10]. Patek SN, Nowroozi BN, Baio JE, Caldwell RL, Summers AP. 2007. Linkage mechanics and power amplification of the mantis shrimp's strike. Journal of Experimental Biology 210:3677–3688.

[11]. Ilton M, Bhamla MS, Ma X, Cox SM, Fitchett LL, Kim Y, Koh J-s, Krishnamurthy D, Kuo C-Y, Temel FZ. 2018. The principles of cascading power limits in small, fast biological and engineered systems. Science 360(6387).

[12]. Burrows M, Shaw S, Sutton G. 2008. Resilin and chitinous cuticle form a composite structure for energy storage in jumping by froghopper insects. BMC Biology 6(1):41. [PubMed: 18826572]

[13]. Lipson H, & Kurman M (2013). Fabricated: The new world of 3D printing. John Wiley & Sons.

[14]. Benyus JM (1997). Biomimicry: Innovation inspired by nature.

[15]. Li B, Haynie DT, Palath N, & Janisch D (2005). Nanoscale biomimetics: Fabrication and optimization of stability of peptide-based thin films. Journal of nanoscience and nanotechnology, 5(12), 2042–2049. [PubMed: 16430138]

[16]. Karlsson M, Davidson M, Karlsson R, Karlsson A, Bergenholtz J, Konkoli Z & Orwar O (2004). Biomimetic nanoscale reactors and networks. Annu. Rev. Phys. Chem, 55, 613–649. [PubMed: 15117264]

[17]. Marino A, Filippeschi C, Mattoli V, Mazzolai B, & Ciofani G (2015). Biomimicry at the nanoscale: current research and perspectives of two-photon polymerization. Nanoscale, 7(7), 2841–2850. [PubMed: 25519056]

[18]. Esfand R, & Tomalia DA (2001). Poly (amidoamine)(PAMAM) dendrimers: from biomimicry to drug delivery and biomedical applications. Drug discovery today, 6(8), 427–436. [PubMed: 11301287]

[19]. Carman ML, Estes TG, Feinberg AW, Schumacher JF, Wilkerson W, Wilson LH,& Brennan AB (2006). Engineered antifouling microtopographies–correlating wettability with cell attachment. Biofouling, 22(1), 11–21. [PubMed: 16551557]

[20]. Snell-Rood E (2016). Bring biologists into biomimetics: engineers, chemists and others taking inspiration from biological systems for human applications must team up with biologists. Nature, 529(7586), 277–279. [PubMed: 26791704]

[21]. Pawlyn M (2011). Biomimicry in architecture (Vol. 15). London: Riba Publishing.

[22]. Yang J, Yao J, Ma Y (2021). A highly flexible, renewable and green alginate polymer for electroactive biological gel paper actuators reinforced with a double-side casting approach. Cellulose, 28, 3647–3662.

[23]. Yang J, Yao J, Guan S (2020). Enhanced electroresponsive and electrochemical poperties of the biological gel artificial muscle prepared by sodium alginate and carboxylated chitosan. Sensors and Actuators B: Chemical, 322.

[24]. Chen J, He C, Gu C, Liu J, Mi C, & Guo S (2014). Compressive and flexural properties of biomimetic integrated honeycomb plates. Materials & Design, 64, 214–220.

[25]. Chen J, Gu C, Guo S, Wan C, Wang X, Xie J, & Hu X (2012). Integrated honeycomb technology motivated by the structure of beetle forewings. Materials Science and Engineering: C, 32(7), 1813–1817. [PubMed: 34062661]

[26]. Gibson LJ, & Ashby MF (1999). Cellular solids: structure and properties. Cambridge University press.

[27]. Yoon SH, Roh JE, & Kim KL (2008). Woodpecker-inspired shock isolation by microgranular bed. Journal of Physics D: Applied Physics, 42(3), 035501.

[28]. May PA, Newman P, Fuster J, & Hirschman A (1976). Woodpeckers and head injury. The Lancet, 307(7957), 454–455.

[29]. Gross BC, Erkal JL, Lockwood SY, Chen C, & Spence DM (2014). Evaluation of 3D printing and its potential impact on biotechnology and the chemical sciences.

[30]. Kodama H (1981). Automatic method for fabricating a three dimensional plastic model with photo hardening polymer. Review of scientific instruments, 52(11), 1770–1773.

[31]. Sachs E, Cima M, Williams P, Brancazio D, & Cornie J (1992). Three dimensional printing: rapid tooling and prototypes directly from a CAD model. Journal of Engineering for Industry, 114(4), 481–488.

[32]. Chia HN, & Wu BM (2015). Recent advances in 3D printing of biomaterials. Journal of biological engineering, 9(1), 4. [PubMed: 25866560]

[33]. Berman B (2012). 3-D printing: The new industrial revolution. Business horizons, 55(2), 155–162.

[34]. Petrick IJ, & Simpson TW (2013). 3D printing disrupts manufacturing: how economies of one create new rules of competition. Research-Technology Management, 56(6), 12–16.

[35]. Mikołajewska E, Macko M, Ziarnecki Ł, Stańczak S, Kawalec P, & Mikołajewski D (2014). 3D printing technologies in rehabilitation engineering.

[36]. Bose S, Vahabzadeh S, & Bandyopadhyay A (2013). Bone tissue engineering using 3D printing. Materials today, 16(12), 496–504.

[37]. Perrot A, Rangeard D, & Pierre A (2016). Structural built-up of cement-based materials used for 3D-printing extrusion techniques. Materials and Structures, 49(4), 1213–1220.

[38]. ASTM Standard D695–15, 2015, "Standard Test Method for Compressive Properties of Rigid Plastics," ASTM International, West Conshohocken, PA, 2015, DOI: 10.1520/D0695-15.

[39]. Cho YH, Lee IH, & Cho DW (2005). Laser scanning path generation considering photopolymer solidification in micro-stereolithography. Microsystem technologies, 11(2–3), 158–167.

[40]. Form 2 – The Most Advanced Desktop 3D Printer Ever Created, Formlabs, [Online] (2017) Available: https://formlabs.com/3d-printers/form-2/ [Accessed 1 June 2018]

[41]. Vella D, Ajdari A, Vaziri A, & Boudaoud A (2012). Indentation of ellipsoidal and cylindrical elastic shells. Physical review letters, 109(14), 144302. [PubMed: 23083246]

[42]. Lazarus A, Florijn HCB, & Reis PM (2012). Geometry-induced rigidity in nonspherical pressurized elastic shells. Physical review letters, 109(14), 144301. [PubMed: 23083245]

[43]. Patek S (2019). The Power of Mantis Shrimp Strikes: Interdisciplanary Impacts of an Extreme Cascade of Energy Release. Integrative and Comparative Biology, 6, 1573–1585.

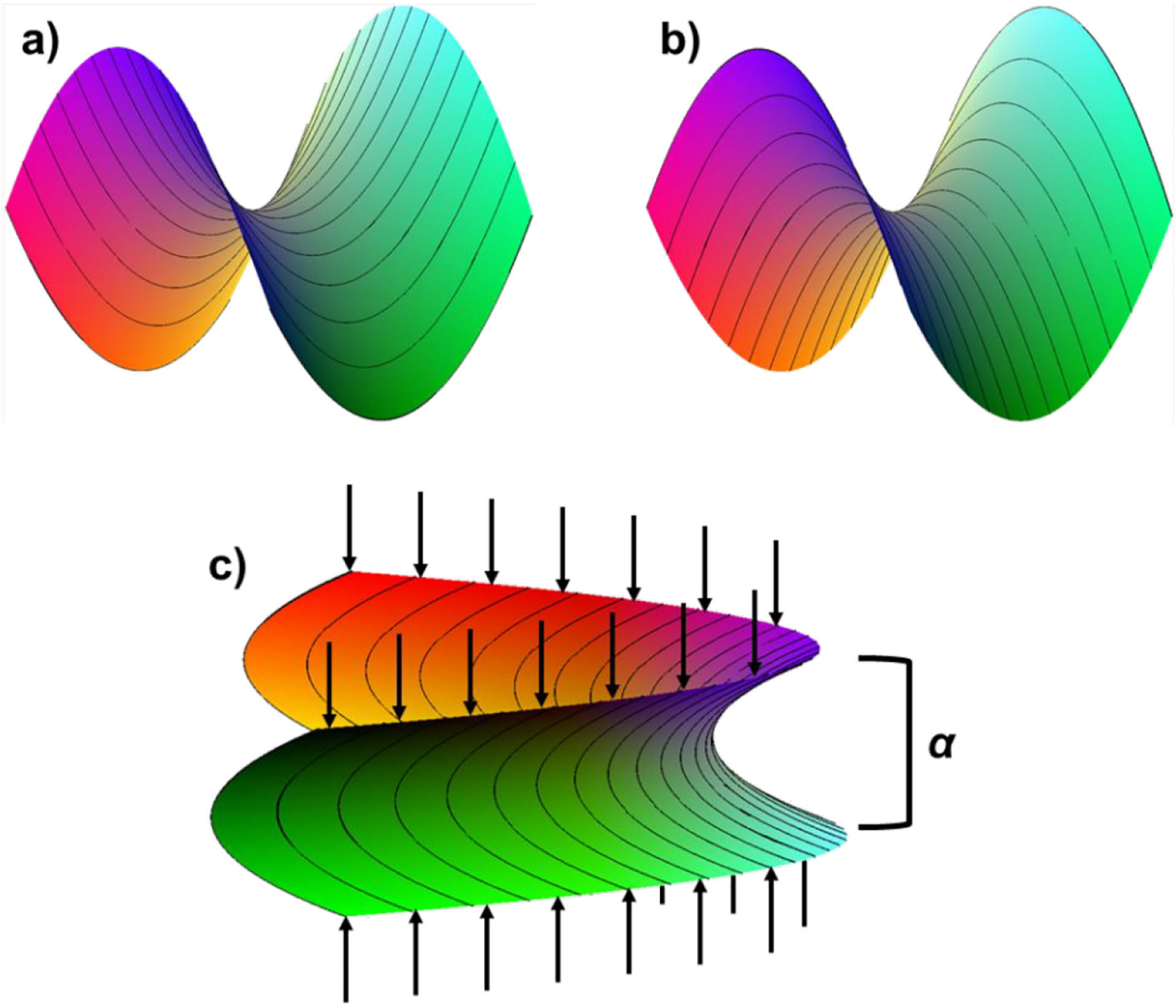

Figure 1.

Representation of saddle print direction for isotropy determination. Lines on the saddles indicate the additive manufacturing print raster direction, either (a) parallel or (b) orthogonal to print direction. (c) Representation of parallel compressive testing.

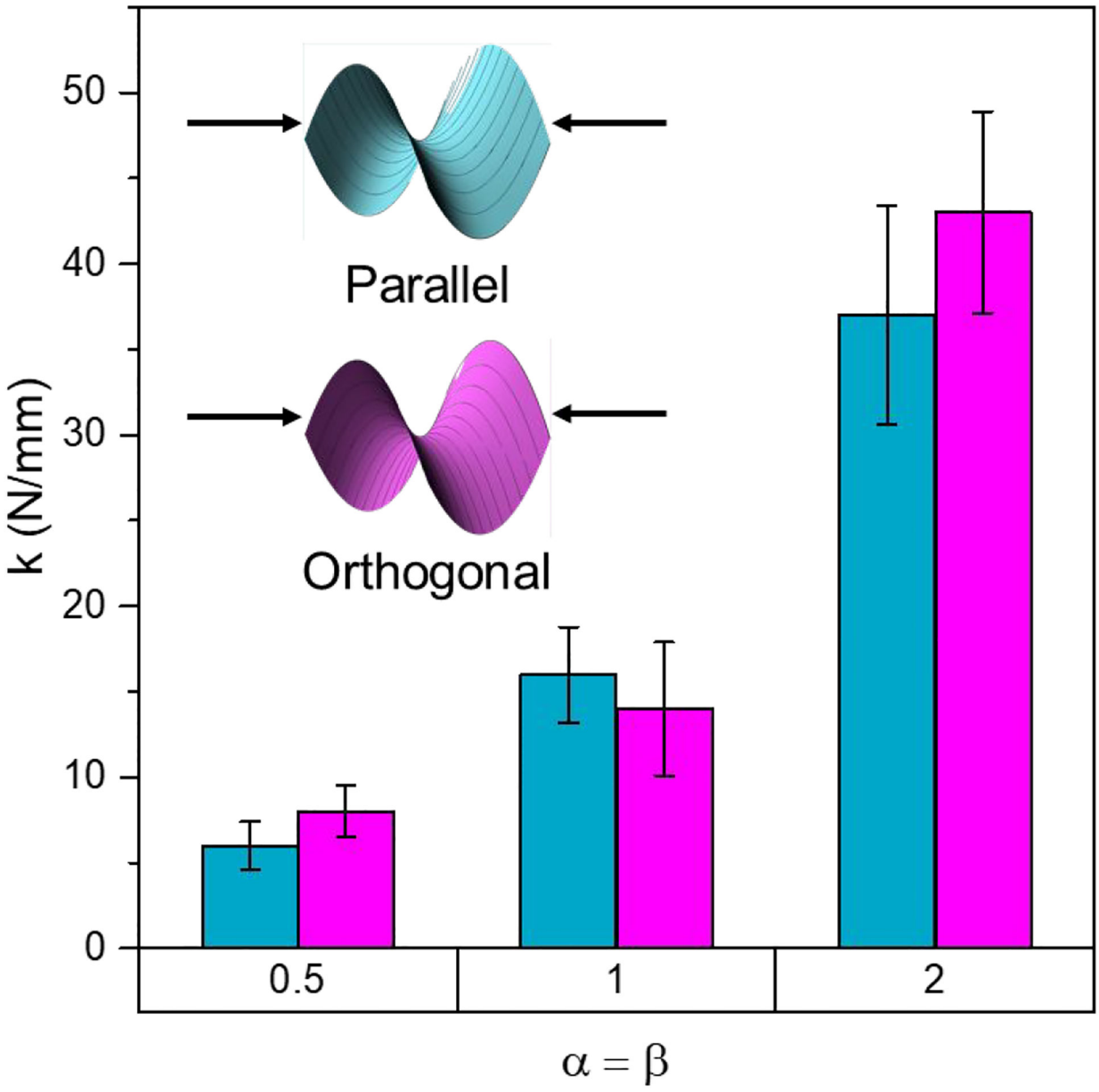

Figure 2.
Spring constants of *stiff* resin saddles indicating isotropy with respect to print raster direction. Arrows shown depict loading direction.

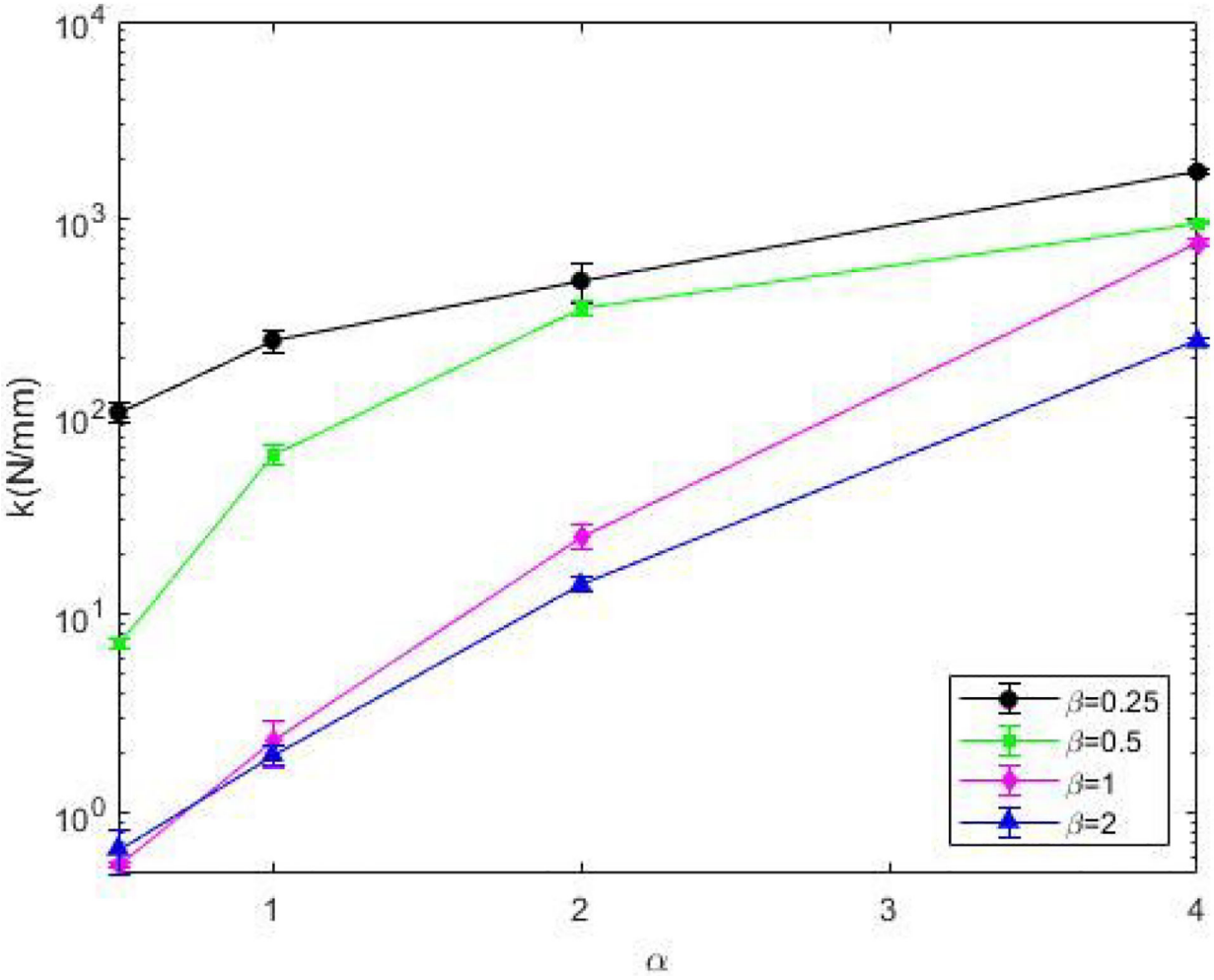

Figure 3.

Comparison of spring constant, *k*, for saddle geometries with differing values of α and β. Note: X-axis starts at 0.5.

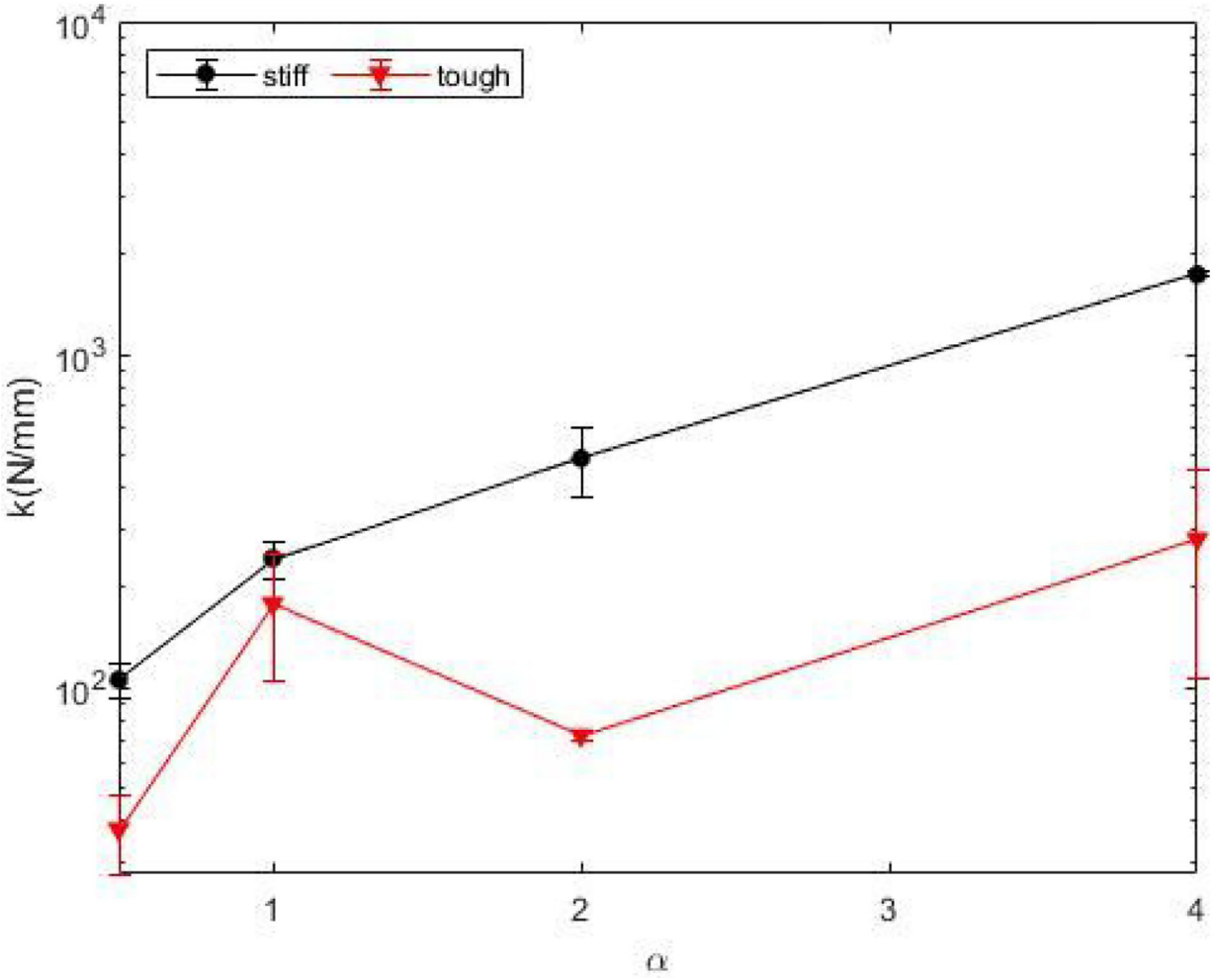

Figure 4.
Comparison of spring constant for the *flexible* and *stiff* resin saddles based on saddle shape (β = 0.25). Note: X-axis starts at 0.5.

Table 1.

Saddle* geometries designed according to Equation 1.

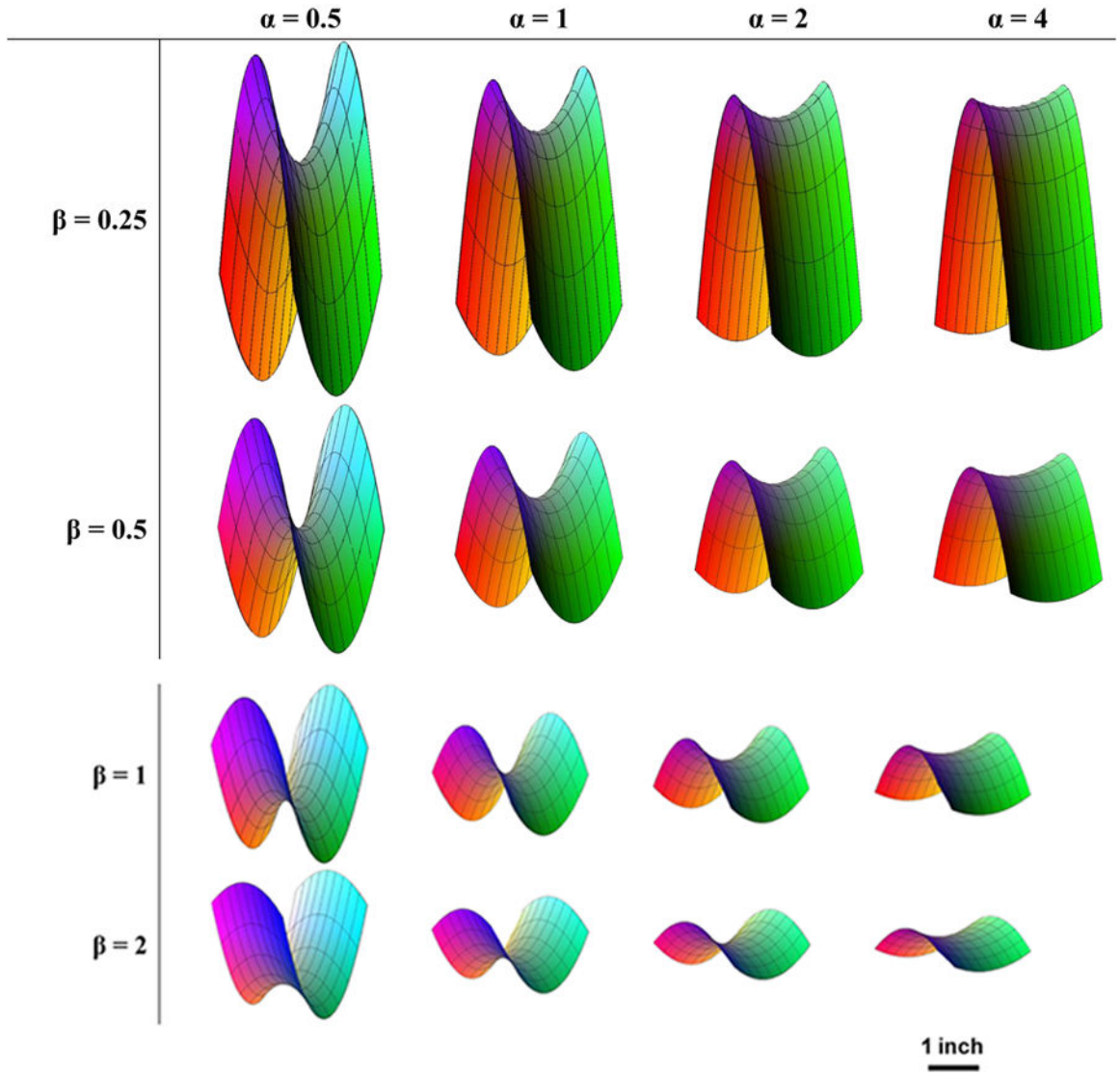

*Each saddle occupies a projected area of 4 square inches.

Table 2.

Summary of spring constants for the *stiff* resin saddles detailed in Table 1.

	Spring Constant, k (N/mm)			
	α = 0.5	**α = 1**	**α = 2**	**α = 4**
β = 0.25	106 ± 12.2	245 ± 31.2	489 ± 115	1740 ± 30.8
β = 0.5	7.21 ± 0.448	65.1 ± 7.94	353 ± 30.8	958 ± 21.6
β = 1	0.543 ± 0.019	2.30 ± 0.626	25.1 ± 3.45	762 ± 28.7
β = 2	0.659 ± 0.165	1.96 ± 0.242	14.2 ± 1.21	241 ± 8.50

Table 3.

A comparison between saddle geometries manufactured with either the *stiff* or *flexible* resin investigated herein. Saddle geometries were manufactured with $\beta = 0.25$ and $\alpha = \{0.5, 1, 2, 4\}$.

	Spring Constant, k (N/mm)			
Resin	$\alpha = 0.5$	$\alpha = 1$	$\alpha = 2$	$\alpha = 4$
stiff	106 ± 12.2	245 ± 31.2	489 ± 115	1740 ± 30.8
flexible	37.7 ± 9.95	179 ± 74.9	72.2 ± 2.25	280 ± 173